Origin of the "0.25 anomaly" in the nonlinear conductance of a quantum point contact

S. Ihnatsenka
Department of Physics, Simon Fraser University, Burnaby, British Columbia, Canada V5A 1S6

I. V. Zozoulenko
Solid State Electronics, ITN, Linköping University, 601 74 Norrköping, Sweden

(Received 25 March 2009; revised manuscript received 8 May 2009; published 10 June 2009)

We calculate the nonlinear conductance of a quantum point contact using the nonequilibrium Green's function technique within the Hartree approximation of spinless electrons. We quantitatively reproduce the "0.25 anomaly" in the differential conductance (i.e., the lowest plateau at $\sim 0.25-0.3\times 2e^2/h$) as well as an upward bending of higher conductance half-integer plateaus seen in the experiments, and relate these features to the nonlinear screening and pinning effects.

DOI: 10.1103/PhysRevB.79.235313 PACS number(s): 73.23.Ad, 71.15.Mb, 71.70.Gm, 73.63.Rt

I. INTRODUCTION

A quantum point contact (QPC) is a narrow constriction of a width comparable to the electron wavelength defined in a two-dimensional electron gas (2DEG) by means of split-gate or etching technique. Due to quantization of the transverse motion electrons can propagate only via allowed modes and the low-temperature linear-response conductance of the QPC shows a steplike dependence on a gate voltage.[1] When a bias voltage V_{sd} is applied between the source and drain electrodes the integer steps in the differential conductance $N\times 2e^2/h$ are smoothed and gradually transformed into the half-integer plateaus $(N-\frac{1}{2})\times 2e^2/h$, where $N=1,2,3,\ldots$ is a number of channels available for propagation.[2–10] Many features of the linear and nonlinear response of the QPC are by now well understood. However, even after 20 years have passed since the discovery of the conductance quantization, some of the important aspects of the QPC conductance are not resolved yet and are still under discussion. One of the prominent examples (apart from the famous "0.7 anomaly"[11]) is a so-called "0.25 feature" in the nonequilibrium differential conductance whose origin is under lively current debate.[8–10]

A theory of the nonequilibrium conductance of the QPC predicting the above mentioned half-integer plateaus was developed by Glazman and Khaetskii.[2] The half-integer plateaus have subsequently been observed and thoughtfully studied by a number of groups.[3–10] The theory of Glazman and Khaetskii[2] and a later more refined approach by Frost *et al.*[5] successfully describe the QPC conductance in the regime when the differential conductance $G_d \gtrsim 2e^2/h$. However, for $G_d \lesssim 2e^2/h$ instead of the expected plateau at $(0.5)\times 2e^2/h$ practically all experiments show a plateau at $(0.2-0.3)\times 2e^2/h$ (sometimes called a 0.25 feature).[3–10] It has been recently argued that the 0.25 feature corresponds to the fully spin polarized current even at zero magnetic field.[10] This conclusion implies far reaching consequences for semiconductor spintronics as it opens up exciting possibilities to generate spin polarized current simply by applying a source-bias voltage to the quantum wire. However, alternative explanations of the 0.25 feature due to the self-consistent electrostatics and nonlinear screening of the lowest *spin-degenerate* subband have been advocated by other groups.[8,9] In particular, Kothari *et al.*[9] demonstrated that the experimental data are well described by the analytical models of Frost *et al.*[5] with phenomenologically introduced asymmetric voltage drop between the source and the drain.

A detailed understanding of the QPC conductance is of prime importance because the QPC represents the cornerstone of mesoscopic physics and the conductance quantization is a fundamental phenomenon of electron transport in low-dimensional structures. The controversy concerning the origin of the 0.25 feature outlines the need for microscopic modeling based on the self-consistent approaches to the electron interaction and nonlinear screening free from adjustable parameters. It should be stressed that previous phenomenological approaches,[2,4,5,9] while providing an important insight for interpretation of experiments, are not, however, able to uncover a microscopic origin of the observed feature.

In this paper we present a model within the self-consistent Hartree approximation that allows us to describe the nonlinear screening and evolution of the conductance plateaus out of equilibrium and thus uncover underlying microscopic origin of the observed features in the differential conductance. To solve the Schrödinger equation we employ a standard nonequilibrium Green's function (NEGF) formalism.[12,13] We demonstrate that for $G\lesssim 2e^2/h$ the differential conductance exhibits $\sim(0.25-0.3)\times 2e^2/h$ plateau (as opposed to the $0.5\times 2e^2/h$ plateau predicted by the noninteracting theories[2,5]). We also find that in the regime of $G\gtrsim 2e^2/h$ the nonlinear screening causes the half-integer plateaus to bend upward as V_{sd} increases. Note that this bending can be clearly seen in all the reported experiments,[3–10] but, surprisingly enough, its presence passed without comments (except for a brief discussion in Ref. 4). Our finding therefore strongly indicates that 0.25 feature is not spin-related and is caused by the nonlinear screening and related pinning of spin-degenerate electrons in the QPC.

II. MODEL

We consider a QPC defined by split gates in a GaAs heterostructure; see Fig. 1. The Hamiltonian of the whole system (the QPC plus the semi-infinite leads) can be written in

the form $H(\mathbf{r})=-\frac{\hbar^2}{2m^*}\nabla^2+V_{\text{eff}}(\mathbf{r})$, where $\mathbf{r}=(x,y)$, $m^*=0.067m_e$ is the GaAs effective mass. The effective potential,

$$V_{\text{eff}}(\mathbf{r}) = V_{\text{conf}}(\mathbf{r}) + V_H(\mathbf{r}) + V_{\text{bias}}(\mathbf{r}), \quad (1)$$

is the sum of the electrostatic confinement (including contributions from the top gates, the donor layer, and the Schottky barrier), the Hartree and the bias potentials (see Ref. 14 for details). We disregard the effect of disorder. The Hartree potential is written in a standard form[14,15] $V_H(\mathbf{r})=\frac{e^2}{4\pi\varepsilon_0\varepsilon_r}\int d\mathbf{r}' n(\mathbf{r}')(\frac{1}{|\mathbf{r}-\mathbf{r}'|}-\frac{1}{\sqrt{|\mathbf{r}-\mathbf{r}'|^2+4b^2}})$, where $n(\mathbf{r})$ is the electron density, $\varepsilon_r=12.9$ is the dielectric constant of GaAs, and the second term describes the mirror charges placed at the distance b from the surface, Fig. 1. The integration is performed over the whole device area including the semi-infinite leads; e.g., the Coulomb interaction is included both in the leads and in the QPC regions.

The Fermi energies E_F in the left (L) and right (R) leads are shifted by the applied source-drain voltage V_{sd}, $E_F^L=E_F^R+eV_{sd}$, while there is a linear ramp of $V_{\text{bias}}(\mathbf{r})$ over the device region[13] (we set $E_F^R=0$). For a finite bias the electric current is calculated as[15] $I=\frac{2e}{h}\int dE\ T(E)[f_L^{\text{FD}}(E)-f_R^{\text{FD}}(E)]$, with $T(E)$ being the transmission coefficient and $f_{L(R)}^{\text{FD}}(E)$ is the Fermi-Dirac (FD) distribution in the left (right) leads. To calculate $T(E)$, the electron density and the local density of states (LDOS) we use the standard NEGF method[12,13] (see the Appendix for the details of our calculations). Having calculated the current I we are in position to calculate the conductance $G=I/V_{sd}$ and the differential conductance $G_d=dI/dV_{sd}$. The latter we compute by increasing the bias voltage slightly and calculating the derivative dI/dV_{sd} numerically.

To outline the role of quantum-mechanical effects in the electron-electron interaction in the QPC, we also consider the Thomas-Fermi (TF) approximation solving the standard TF equation to find the effective TF potential[14] and calculating G and G_d for this potential using the NEGF. This approximation does not capture quantum-mechanical quantization of electron motion and, therefore, utilization of the TF approximation is conceptually equivalent to a one-electron noninteracting approach.

III. RESULTS AND DISCUSSION

Figures 1(a) and 1(b) show the conductance G of the QPC calculated within the TF and Hartree approximations for different source-drain voltages V_{sd}. The parameters of the QPC are indicated in Fig. 1 and are chosen close to those typically used in experiments (note that we performed calculations for shorter QPCs which show the same behavior). For zero V_{sd} the conductance shows well-defined quantized plateaus for both TF and Hartree approaches. The latter, however, predicts broader transition regions between the plateaus. The reason is the energy level pinning effect.[14] This is illustrated in Figs. 1(c) and 1(d) that show the resonant energy structure inside the QPC constriction (i.e., the position of the peak in the LDOS integrated over the geometrical area of the QPC constriction). In the TF approach the resonant levels sweep past E_F in a linear fashion. In contrast, the Hartree calculations show pinning of the energy levels [corresponding to the one-dimensional (1D) subbands in the narrowest part of the constriction] to E_F within the energy window $\pm 2\pi k_B T$. Within this window the FD distribution $0<f^{\text{FD}}<1$ and thus the states are only partially filled. This leads to metallic-like behavior when electrons can be easily rearranged to screen

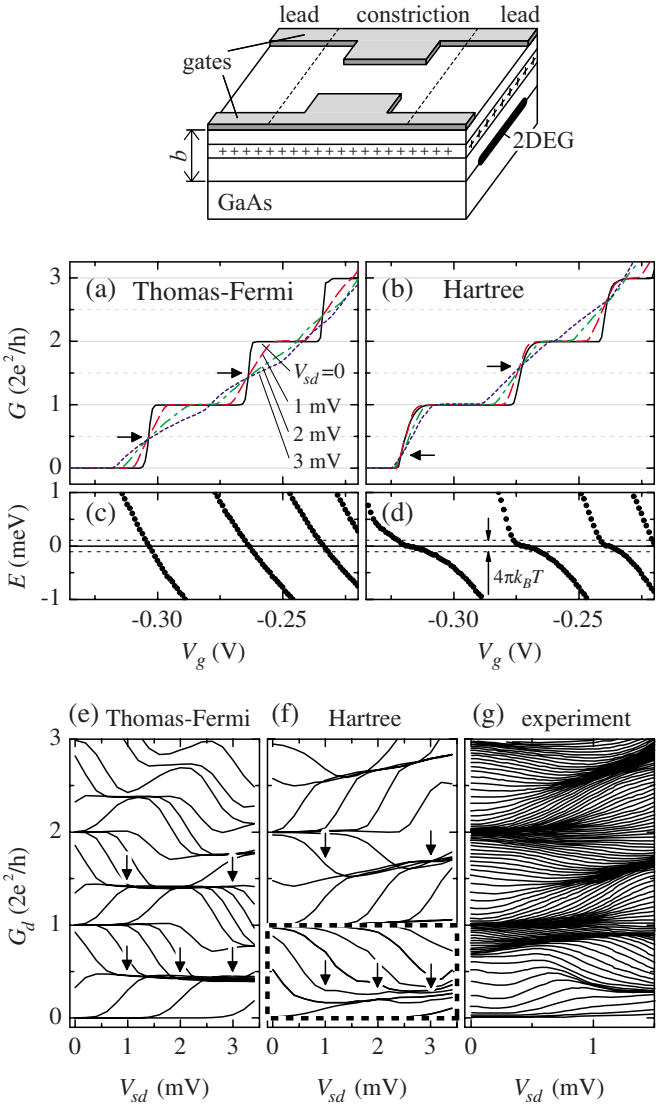

FIG. 1. (Color online) [(a) and (b)] Conductance G of the QPC calculated within the TF and Hartree approximations for different bias voltages V_{sd}. [(c) and (d)] Resonant energy structure (i.e., the LDOS integrated over the geometrical area of the QPC constriction) in equilibrium, $V_{sd}=0$. [(e) and (f)] The differential conductance G_d calculated within the TF and Hartree approximations. Traces are taken at different gate voltages with 5 mV step [the dashed rectangular in (f) contains curves with 2.5 mV step]; (g) shows the experientially measured G_d adopted from Ref. 7. The inset on the top illustrates a geometry of the QPC defined in a GaAs heterostructure. A negative voltage is applied to the top gates depleting the 2DEG residing on the distance $b=60$ nm beneath the surface. The widths of the cap, donor, and spacer layers are 14, 36, and 10 nm, respectively; the donor concentration is 0.64×10^{24} m^3. The geometrical width and length of the constriction are, respectively, 60 nm and 400 nm. Temperature $T=0.2$ K.

the external electric field. (For influence of the pinning effect on equilibrium transport in quantum dots see Ref. 14; see also Ref. 16 for the experimental studies of the energy level pinning in the QPC in the magnetic field.)

Out of equilibrium, the energy window eV_{sd} providing current-carrying states increases as the source-drain voltage grows and the conductance plateaus become smeared; see Figs. 1(a) and 1(b). The plateaus in the conductance G completely disappear when eV_{sd} exceeds the 1D subband energy separation inside the QPC constriction. At the same time, half-integer plateaus $(N-\frac{1}{2})\times 2e^2/h$ appear in the differential conductance G_d; see Figs. 1(e) and 1(f). A comparison of the TF and Hartree results shows two profound differences between the calculated G_d. First, the lowest Hartree plateau $N=1$ occurs at $G_d^H \approx 0.25-0.3\times 2e^2/h$ as opposed to the $G_d^{\mathrm{TF}}=0.5\times 2e^2/h$ plateau predicted by the TF calculations. Second, all TF plateaus are flat and rather independent of V_{sd}, whereas all higher Hartree plateaus $N\geq 2$ are bent upward as V_{sd} increases. Note that these two features of the calculated G_d^H are clearly seen in all reported experiments[3–10] [see Fig. 1(g) for a representative example].

In order to understand the origin of the above features of the QPC nonlinear conductance let us inspect the LDOS inside the QPC region. Let us first concentrate at the first plateau in the differential conductance. Figures 2(c), 2(e), and 2(g) show the evolution of LDOS as V_{sd} is increased calculated within the noninteracting TF approach. The enhanced LDOS in the constriction corresponds to the position of the bottom of the lowest propagating subband. In the TF approximation the effective confinement potential is symmetrically distributed relative to V_{bias} (that ramps linearly along the device). Because of this the 1D subband touches V_{bias} at the QPC center (at the energy $E=E_F^L-\frac{eV_{sd}}{2}$). As a result, the electrons injected from the left lead in the upper half of the eV_{sd} window $(E_F^L<E<E_F^L-\frac{eV_{sd}}{2})$ pass through the QPC with the unit probability. However, the electrons in the lower half of the eV_{sd} window experience a potential barrier and hence are reflected back [see partial current profiles, $T(E)[f_L^{\mathrm{FD}}(E)-f_R^{\mathrm{FD}}(E)]$, in small insets in Figs. 2(c), 2(e), and 2(g)]. Thus, the electrons injected from the left lead give rise to the conductance of the half of the conductance unit, $G_d=0.5\times 2e^2/h$. For electrons moving in the opposite direction, from the drain to the source electrode, there is no available channel to propagate and all of them are reflected.

A character of electron transport changes dramatically when interaction is included at the level of the quantum-mechanical Hartree approach. Figures 2(d), 2(f), and 2(h) show the LDOS inside the constriction calculated within the Hartree approximation for the first half-integer plateau where $G_d\approx 0.3\times 2e^2/h$. With one partially propagating mode the electron density inside the constriction is low and the screening is rather weak, and hence the electron interaction strongly modifies the potential profile in comparison to the symmetric TF distribution. The Coulomb charging pushes up the upper 1D subband inside the QPC constriction to the top of the eV_{sd} window near the source contact. (It is interesting to note that the LDOS inside the QPC out of equilibrium resembles a corresponding self-consistent LDOS profile of a resonant-tunneling diode.[17]) Thus, the 1D subbands become

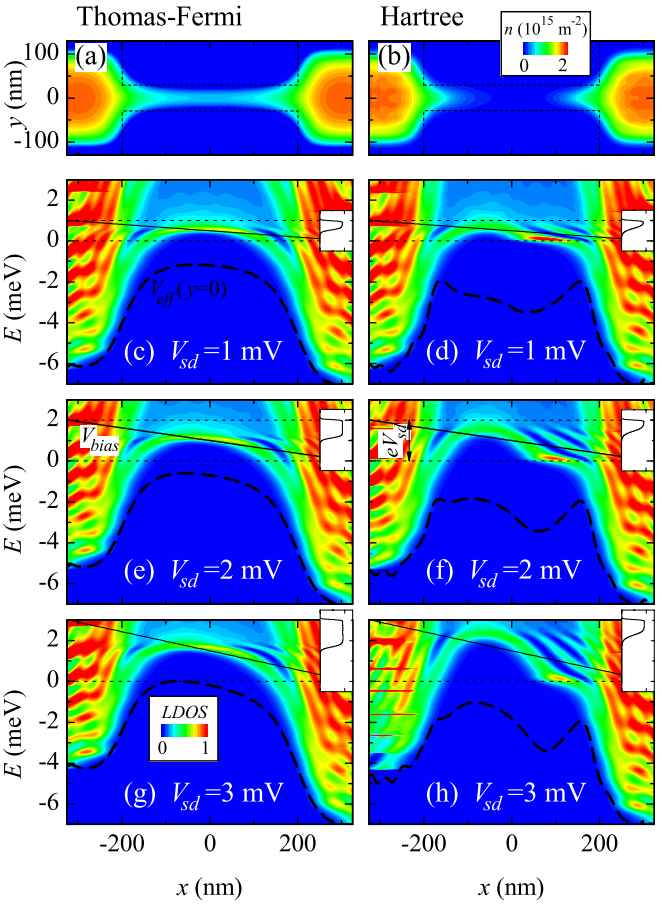

FIG. 2. (Color online) The charge density and the LDOS of the QPC calculated in the Thomas-Fermi and Hartree approximations (left and right panels, respectively) for the first half-integer plateau for different V_{sd}. The corresponding gate voltages V_g are marked by arrows in Figs. 1(a), 1(b), 1(e), and 1(f). The effective potential Eq. (1) is plotted by the dashed lines. Solid slanted lines denote the bias potential profile V_{bias}. Insets show the current profiles, $T(E)[f_L^{\mathrm{FD}}(E)-f_R^{\mathrm{FD}}(E)]$.

pinned to the top of the eV_{sd} window and therefore only a relatively narrow energy interval can supply current-carrying states that pass through the QPC [see current profiles in the insets of Figs. 2(d), 2(f), and 2(h)]. Hence, the QPC conductance, $G_d\approx 0.3\times 2e^2/h$, becomes smaller than a half of the conductance unit $G_0=2e^2/h$. Our calculations provide therefore a microscopic foundation of the phenomenological approaches that describe the 0.25 anomaly assuming a nonsymmetric voltage drop inside the constriction.[5,9]

Let us now turn to higher half-integer plateaus. In this case there is at least one propagating state inside the constriction, which, in turn, leads to enhanced screening. Indeed, despite the voltage drop between the left and the right leads, the Hartree effective potentials V_{eff} and the LDOS are practically flat inside the QPC; see Figs. 3(b) and 3(d). This is in contrast to the corresponding TF results which do not account for screening and thus follow the linear drop of V_{bias}; see Figs. 3(a) and 3(c). Because of the enhanced screening, at the center of the QPC the Hartree 1D subbands are situated lower than the corresponding TF subbands (i.e., below $E_F^L-\frac{eV_{sd}}{2}$), and hence the energy window providing the trans-

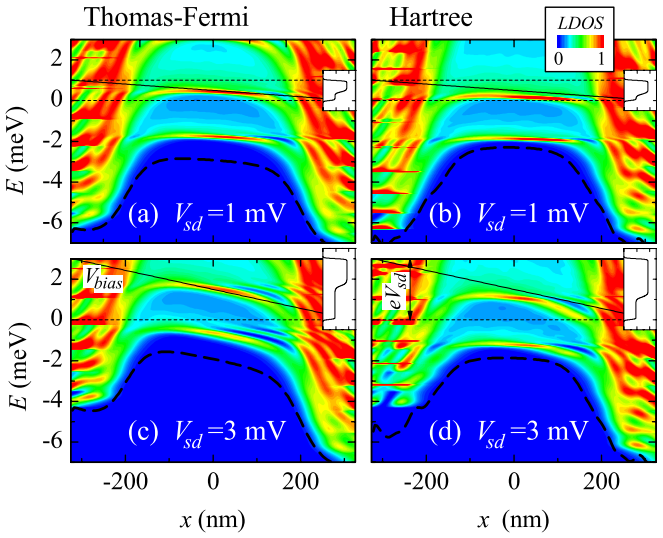

FIG. 3. (Color online) TF and Hartree LDOS in the QPC for different V_{sd}. [The same as in Fig. 2 but for the second half-integer plateau in the differential conductance, see arrows at Figs. 1(a), 1(b), 1(e), and 1(f).]

mitted states through the QPC exceeds the half of the available energy interval eV_{sd} [see the current profiles in the inset of Figs. 3(b) and 3(d)]. As a result, the QPC conductance corresponding to the highest subband is larger than a half of the conductance unit G_0. (Note that all lower subbands are fully occupied and thus contribute to one conductance unit each.) Thus, the enhanced screening, which becomes more pronounced as V_{sd} increases, is the reason for the upward bending of the higher half-integer plateaus.

Finally, we stress that we utilized a model of *spinless* electrons in the Hartree approximation. The present approach can be easily extended to account for the spin effect within the framework of the spin-density functional theory (SDFT). However, some previous studies questioned the reliability of the SDFT for the system at hand because of the self-interaction errors of the local spin-density approximation.[18] Hence, the definite answer about the role of the spin in the nonlinear conductance of the QPC might require approaches that go beyond the mean-field method used in the present study (e.g., quantum Monte Carlo, etc.). At the same time, an excellent quantitative agreement of our calculations with the experimental results outlines the dominant role of the self-consistent electrostatics and the nonlinear screening and strongly indicates that the 0.25 feature is not spin-related. We note also its generic property because calculations for QPC of different lengths and widths give the same qualitative behavior.

To conclude, using NEGF formalism within the Hartree model of spinless electrons we reproduced quantitatively the observed features of the nonlinear QPC conductance and provide microscopic interpretation of the 0.25 anomaly as well as the upward bending of the higher half-integer plateaus in terms of nonlinear screening and pinning effect.

ACKNOWLEDGMENTS

This work was supported by the Swedish Research Council (VR).

APPENDIX: NEGF TECHNIQUE FOR CALCULATION OF THE TRANSMISSION COEFFICIENT OF THE QPC

The central quantity in the NEGF is the lesser Green's function $G^<$ (Ref. 12). To calculate it one has to find first the retarded Green's function, G^r,

$$[E - H(\mathbf{r})]G^r(\mathbf{r},\mathbf{r}',E) = \mathbf{1}, \tag{A1}$$

where E is an electron energy and $\mathbf{1}$ is the unitary operator. This equation can be reformulated using the so-called retarded self-energies of the leads, Σ_R^r and Σ_L^r,

$$[E - H_0 - \Sigma_R^r(E) - \Sigma_R^r(E)]G^r(E) = \mathbf{1}, \tag{A2}$$

where H_0 is the Hamilton operator for the isolated scattering region (i.e., excluding the leads). (For the sake of shortness we will not write explicitly a coordinate dependence of G^r). $\Sigma_{R(L)}^r$ are functions with nonzero values only at the boundaries with the semi-infinitive leads. Coupling the scattering region with leads is described by the functions

$$i\Gamma_R(E) = \Sigma_R^r(E) - \Sigma_R^a(E) = 2i\ \mathrm{Im}[\Sigma_R^r(E)], \tag{A3a}$$

$$i\Gamma_L(E) = \Sigma_L^r(E) - \Sigma_L^a(E) = 2i\ \mathrm{Im}[\Sigma_L^r(E)]. \tag{A3b}$$

The lesser Green's function in the scattering region is related to electron flow from right and left reservoirs and is written as

$$G^<(E) = -if_R^{\mathrm{FD}}(E)G^r(E)\Gamma_R(E)G^a(E) - if_L^{\mathrm{FD}}(E)G^r(E)\Gamma_L(E)G^a(E), \tag{A4}$$

where $f_{R(L)}^{\mathrm{FD}}$ are the Fermi-Dirac functions in the right (left) lead. This equation has to be used in nonequilibrium situations when $V_{sd} \neq 0$ and $f_R^{\mathrm{FD}} \neq f_L^{\mathrm{FD}}$. In equilibrium, when the Fermi functions in both leads are identical, Eq. (A4) reduces to

$$G_{\mathrm{eq}}^<(E) = 2f_{R(L)}^{\mathrm{FD}}(E)G^r(E). \tag{A5}$$

It is also valid under a bias voltage at energies E for which $f_R^{\mathrm{FD}} = f_L^{\mathrm{FD}}$ (in practice, $f_{R(L)}^{\mathrm{FD}} = 1$ for those energies).

In order to calculate the electron density we integrate over the electron energy E,

$$n(\mathbf{r}) = -\frac{1}{2\pi}\int dE\ \mathrm{Im}[G^<(\mathbf{r},\mathbf{r},E)]. \tag{A6}$$

We use both Eqs. (A4) and (A5) to perform this integration. $G_{\mathrm{eq}}^<(E)$, Eq. (A5), is analytic in the upper half of the imagi-

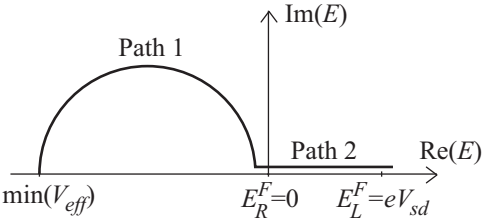

FIG. 4. An integration path used in Eq. (A6). Path 2 appears when the bias voltage V_{sd} is applied.

nary plane whereas $G^{<}(E)$, Eq. (A4), has poles below and above the real E axis. Thus, for the energies when $f^{\mathrm{FD}}_{R(L)}=1$ we can use $G^{<}_{\mathrm{eq}}(E)$ for which we can transform the integration path from the real axis to the complex plane,[19] see Fig. 4, where $G^{<}_{\mathrm{eq}}(E)$ is a smooth function of energy. The rest of the integration (i.e., path 2 in Fig. 4(b) where $f^{\mathrm{FD}}_{R(L)}\neq 1$) is close to the real axis and there Eq. (A4) is used. Along the path 1 only several integration points are needed because the rapid variations of $G^{<}_{\mathrm{eq}}(E)$ are smeared out when the integration path is far from the real axis. This is especially useful for the bound states, which give rise to sharp peaks near the real axis. On the straight path along the real axis, one needs much more integration points and for large source-drain voltage it becomes the most time consuming part of computation.

Equations (A1), (A2), and (A4)–(A6) are solved self-consistently in an iterative way until a converged solution for the electron density and potential (and hence for the total Green's function) is obtained. Having calculated the total self-consistent Green's functions, the transmission coefficient is calculated as[12]

$$T(E)=\mathrm{Tr}[\Gamma_L(E)G^r(E)\Gamma_R(E)G^a(E)]. \tag{A7}$$

To speed up computation we employ the hybrid recursive method working with sin-Fourier transformed Green's functions[20] and use the second Broyden method for the iterative algorithm.[21]

[1] D. A. Wharam, T. J. Thornton, R. Newbury, M. Pepper, H. Ahmed, J. E. F. Frost, D. G. Hasko, D. C. Peacock, D. A. Ritchie, and G. A. C. Jones, J. Phys. C **21**, L209 (1988); B. J. van Wees, H. van Houten, C. W. J. Beenakker, J. G. Williamson, L. P. Kouwenhoven, D. van der Marel, and C. T. Foxon, Phys. Rev. Lett. **60**, 848 (1988).

[2] L. I. Glazman and A. V. Khaetskii, Pis'ma Zh. Eksp. Teor. Fiz. **48**, 546 (1988).

[3] N. K. Patel, J. T. Nicholls, L. Martin-Moreno, M. Pepper, J. E. F. Frost, D. A. Ritchie, and G. A. C. Jones, Phys. Rev. B **44**, 13549 (1991).

[4] L. Martin-Moreno, J. T. Nicholls, N. K. Patel, and M. Pepper, J. Phys.: Condens. Matter **4**, 1323 (1992).

[5] J. E. F. Frost, K.-F. Berggren, M. Pepper, M. Grimshaw, D. A. Ritchie, A. C. Churchill, and G. A. C. Jones, Phys. Rev. B **49**, 11500 (1994).

[6] A. Kristensen, H. Bruus, A. E. Hansen, J. B. Jensen, P. E. Lindelof, C. J. Marckmann, J. Nygård, C. B. Sørensen, F. Beuscher, A. Forchel, and M. Michel, Phys. Rev. B **62**, 10950 (2000).

[7] S. M. Cronenwett, H. J. Lynch, D. Goldhaber-Gordon, L. P. Kouwenhoven, C. M. Marcus, K. Hirose, N. S. Wingreen, and V. Umansky, Phys. Rev. Lett. **88**, 226805 (2002).

[8] R. de Picciotto, L. N. Pfeiffer, K. W. Baldwin, and K. W. West, Phys. Rev. Lett. **92**, 036805 (2004).

[9] H. Kothari, A. Ramamoorthy, R. Akis, S. M. Goodnick, D. K. Ferry, J. L. Reno, and J. P. Bird, J. Appl. Phys. **103**, 013701 (2008).

[10] T.-M. Chen, A. C. Graham, M. Pepeper, I. Farrer, and D. A. Ritchie, Appl. Phys. Lett. **93**, 032102 (2008).

[11] K. J. Thomas, J. T. Nicholls, M. Y. Simmons, M. Pepper, D. R. Mace, and D. A. Ritchie, Phys. Rev. Lett. **77**, 135 (1996); for a review of different theoretical approaches to this effect see, e.g., *0.7 Feature & Many-Body Phenomena in One-Dimensional Conductors*, special issue of J. Phys.: Condens. Matter **20** (2008).

[12] S. Datta, *Electronic Transport in Mesoscopic Systems* (Cambridge University Press, Cambridge, 1997).

[13] Y. Xue, S. Datta, and M. A. Ratner, Chem. Phys. **281**, 151 (2002).

[14] S. Ihnatsenka, I. V. Zozoulenko, and M. Willander, Phys. Rev. B **75**, 235307 (2007); S. Ihnatsenka and I. V. Zozoulenko, Phys. Rev. Lett. **99**, 166801 (2007).

[15] J. Davies, *The Physics of Low-Dimensional Semiconductors* (Cambridge University Press, Cambridge, UK, 1998).

[16] A. C. Graham, D. L. Sawkey, M. Pepper, M. Y. Simmons, and D. A. Ritchie, Phys. Rev. B **75**, 035331 (2007).

[17] G. Klimeck, R. Lake, R. C. Bowen, W. R. Frensley, and T. S. Moisea, Appl. Phys. Lett. **67**, 2539 (1995).

[18] S. Ihnatsenka and I. V. Zozoulenko, Phys. Rev. B **76**, 045338 (2007).

[19] S. Ihnatsenka and I. V. Zozoulenko, Phys. Rev. B **73**, 075331 (2006).

[20] I. V. Zozoulenko, F. A. Maaø, and E. H. Hauge, Phys. Rev. B **53**, 7975 (1996); **53**, 7987 (1996).

[21] G. Broyden, Math. Comput. **19**, 577 (1965); D. Singh, H. Krakauer, and C. S. Wang, Phys. Rev. B **34**, 8391 (1986).